ACS APPLIED MATERIALS & INTERFACES

Forum Article

www.acsami.org

Nanoporous Thin Films and Binary Nanoparticle Superlattices Created by Directed Self-Assembly of Block Copolymer Hybrid Materials

Torsten Pietsch,*[,†,‡] Peter Müller-Buschbaum,[§] Boris Mahltig,[⊥] and Amir Fahmi*[,†,#]

[†]Manufacturing Division, Faculty of Engineering, University of Nottingham, University Park, Nottingham NG7 2RD, United Kingdom

[§]Physik-Department, Lehrstuhl für Funktionelle Materialien, Technische Universität München, James-Franck-Straße 1, 85748 Garching, Germany

[⊥]Faculty of Textile and Clothing Technology, Niederrhein University of Applied Sciences, Webschulstrasse 31, 41065 Mönchengladbach, Germany

ABSTRACT: The design and development of well-defined, functional nanostructures via self-assembly is one of the key objectives in current nanotechnology. Block copolymer-based hybrid materials are attractive candidates for the fabrication of multifunctional nanostructures, which provide the building blocks for more complex nanoarchitectures and nanodevices. However, one of the major challenges lies in controlling the structure formation in these hybrid materials by guiding the self-assembly of the block copolymer. Here, hierarchical nanoporous structures are fabricated via guided multistep self-assembly of diblock copolymer micellar solutions onto hydrophilic solid substrates. The core of polystyrene-*block*-poly[4-vinylpyridine] micelles serves as a nanoreactor for the preparation of size-controlled gold nanoparticles. Deposition of thin films of the micellar solution in combination with a nonselective cosolvent (THF), on hydrophilic surfaces leads to the formation of hierarchical nanoporous structures. The micellar films exhibit two different pore diameters and a total pore density of more than 10^{10} holes per cm^2. Control over the pore diameter is achieved by adapting the molecular weight of the polystyrene-*block*-poly[4-vinylpyridine] diblock copolymer. Moreover, the porous morphology is used as a template for the fabrication of bimetallic nanostructured thin films. The PS-*b*-P4VP template is subsequently removed by oxygen plasma etching, leaving behind binary nanoparticle structures that mimic the original thin film morphology.

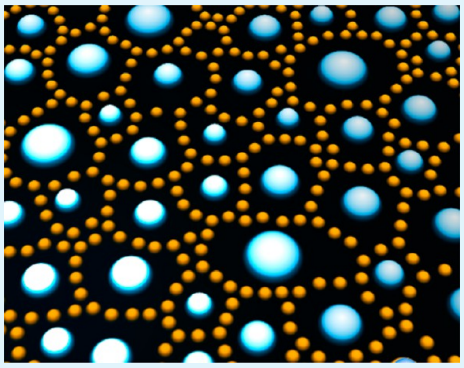

KEYWORDS: *block copolymer, bimetallic, hybrid materials, micelle, nanofabrication, nanoparticle, self-assembly, thin films*

INTRODUCTION

Nanoporous inorganic films have attracted considerable interest because of their wide range of different applications in antireflective coatings,[1,2] catalysis,[3] membranes,[4,5] sensors,[5−8] and electronic devices.[9,10] Typically, such films were prepared by post-deposition treatment methods including UV-,[8] acid-[11] and solvent-etching[2] as well as emulsion templating.[12,13] For example, antireflective coatings have been realized by combining hollow silica nanoparticles and mesoporous silica nanosheets,[14] creating double-nanotextured surfaces[15] and self-assembling moth eyes pattern.[16] Such coatings will be useful for devices such as solar cells or as screen coatings. Another important type of application of nanoporous inorganic films is catalysis, which typically requires metallic nanoparticles with a very controlled size and size distribution.[17−19] In this area, especially bimetallic nanoparticles containing the metals gold, platinum and cobalt are presented in literature.[20−23] For example nanoporous Cu−Pt(Pd) core−shell structure for application in electrocatalysis were synthesized by galvanic replacement by Xu et al.[24]

Recently, Russell and co-workers demonstrated that nanoparticles can be selectively incorporated within cylindrical diblock copolymer nanodomains, which are formed via self-assembly.[25−27] A similar concept to generate nanostructures of metal and metal-oxide in self-assembled block copolymer matrix was developed by Gutmann et al.[28] Such control on the nanoscopic level represents a significant advance in directing the order of nanoparticles into self-assembled matrices. However, Möller et al.[29] provided a much simpler concept to produce hexagonal arrays of gold nanodots on solid substrates based on dip-coating of micelles containing ultrasmall gold nanoparticles. This technique can also be used to fabricate inorganic nanoporous compounds using a compact self-assembled template of block copolymer micelles.[30] Recently,

Special Issue: Forum on Polymeric Nanostructures: Recent Advances toward Applications

Received: October 31, 2014
Accepted: February 3, 2015
Published: February 3, 2015

DOI: 10.1021/am5076056
ACS Appl. Mater. Interfaces 2015, 7, 12440−12449

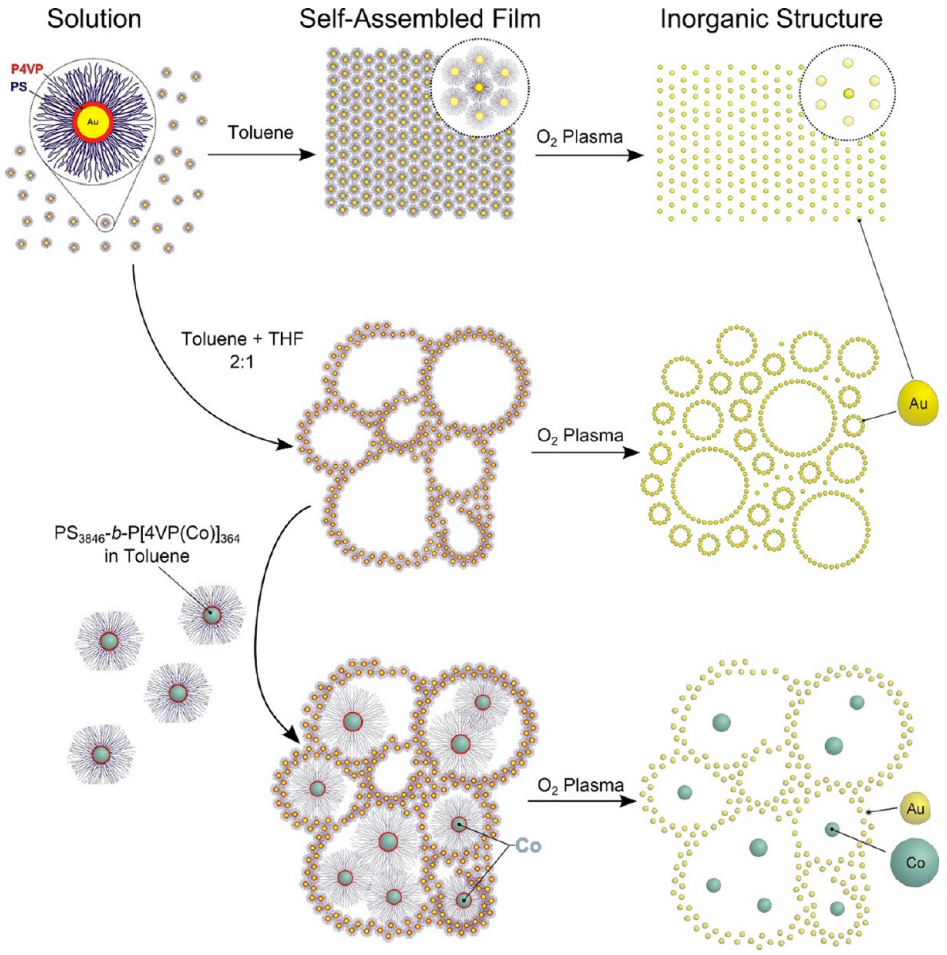

Figure 1. Schematic illustration of the fabrication of bimetallic structures via directed self-assembly of nanoparticle loaded PS-*b*-P4VP block copolymer micelles. First, micelles incorporating Au-nanoparticles in their core (P4VP) are prepared in toluene solution. The micelle's core provides a confined environment for the synthesis of inorganic nanoparticles with low polydispersity. Additionally, the block copolymer stabilizes the nanoparticles in organic media. After adding a nonselective cosolvent (THF), nanoporous thin films are prepared by spin-coating micelles from toluene-THF solution onto hydrophilic substrates. Nanoporous assemblies of gold nanoparticles, which mimic the original thin film morphology, are obtained after the copolymeric matrix is removed by oxygen plasma etching. Alternatively, large micelles of PS-*b*-P4VP incorporating a second type of nanoparticles (e.g., Co) are deposited into the porous template. Hence, after the removal of the organic PS-*b*-P4VP matrix via oxygen plasma etching, ordered bimetallic arrays of Au and Co nanoparticles are obtained.

it was presented that the self-assembly of such micellar block-copolymer hybrid materials can be guided by accurately controlling the polymer properties, such as molecular weight, volume fraction, and chemical composition, as well as processing condition as well as the composition of the casting solution.[31−33] For instance, the interfacial energy of the core/corona interface and entropy loss are due to the aggregation of insoluble blocks into ordered microdomains.[34] In thin film, additional parameters, e.g., the balance of forces between coronal chains and substrate surface interactions, also play an important role.[35] Indeed, fine-tuning the scale and morphology of self-assembled nanostructures requires control over chemical composition and architecture of the copolymer as well as the solution conditions (concentration, temperature, polarity etc.).[36−38] This control scheme can also be exploited to fabricate well-defined nanostructures of inorganic materials.[30,31,39] For example, recently Peinemann and co-workers developed a versatile approach to fabricate ultrananoporous compounds with precisely controllable pore-size based on the deposition of inverse block copolymer micelles, which are functionalized via the incorporation of inorganic nanoparticles.[40,41]

In the present work, we demonstrate the controlled fabrication of very thin porous films and bimetallic nanoparticle structures via multistep guided self-assembly of block copolymer based hybrid materials. Such controlled nanostructured surfaces and films will be highly interesting for applications as outlined above. This study focuses on the fabrication of nanoporous thin films by combining self-assembly of hybrid materials,[42] as shown in Figure 1, in combination with a templating approach to fabricate complex bimetallic structure. Because of the nature of this process, no additional treatments are necessary to develop the pores, which is one of the major limitations of conventional methods. The application of block copolymer micelles to template inorganic nanoparticles (NPs) in their core is advantageous because of the possibility to achieve control over the size and polydispersity of the nanoparticles. The basic function of the block copolymers is to form steric- or ionic barriers around the nanoparticles to prevent aggregation and precipitation.[43] Moreover, the possibility to self-assemble into a variety of patterns adds another important function.

The novelty of this work resides in the combination of two outstanding factors. First, gold nanoparticles (<5 nm) were

DOI: 10.1021/am5076056
ACS Appl. Mater. Interfaces 2015, 7, 12440−12449

generated with a very narrow size distribution. The high control of the size distribution will be extremely beneficial for applications among catalysis. Second, the design and fabrication of nanoporous structures was achieved via self-assembly of organic−inorganic hybrid materials without the use of postdeposition treatments such as annealing, substrate surface modification or external fields. These nanoporous thin films can be used as an effective host for other metals to generate nanostructured surface alloys, which have numerous technological applications as well, e.g., in catalysts, optics, electronics, etc.[27,43,44]

EXPERIMENTAL SECTION

Materials. Polystyrene-*block*-polyvinylpyridine copolymers were obtained from Polymer Source Inc. and used as received. Details are listed in Table 1. Metal compounds ($HAuCl_4$, and $CoCl_2$,) used as precursors for the corresponding metals were purchased from Sigma-Aldrich, Riedel-de Haën or Fluka and used as received and all organic solvents were obtained from Fisher Scientific Ltd. and used without further purification. Native oxidized silicon (Si) wafers (⟨111⟩) were purchased from Siltronix; the wafers were cut using a high precision abrasive cutoff machine (model 5085) equipped with a 40 μm wide diamond blade (NBZ-Z 1050 51.2 × 0.045 × 40). After cutting, the Si substrates were rinsed with distilled water and the protective resin was removed with acetone. Subsequently the samples were cleaned using a combination of piranha- H_2SO_4:H_2O_2:H_2O = 2:1:1) at 80 °C for 20 min and RCA-1 cleaning procedure (H_2O_2:NH_4OH:H_2O = 4:1:1) at 60 °C for another 20 min.[45] After rinsing the surface with DI water, the substrates were dried with nitrogen.

Table 1. Properties of PS-b-P4VP Polymers

sample	PS (g/mol)	P4PV (g/mol)	fP4VP	M_w/M_n	D_P (nm)
PS_{398}-*b*-$P4VP_{18}$	41 400	1900	0.04	1.07	2.4 ± 0.6
PS_{3846}-*b*-$P4VP_{364}$	400 000	38 200	0.09	1.37	12.8 ± 2.1
PS_{206}-*b*-$P4VP_{197}$	21 400	20 700	0.49	1.13	3.6 ± 1.5

Nanoparticle Synthesis. First, noble metal nanoparticles (Au, Co/CoO) are selectively incorporated into the P4VP block of polystyrene-*block*-polyvinylpyridine (PS-*b*-P4VP) micelles in toluene via chemical reduction of an inorganic precursor ($HAuCl_4$, $CoCl_2$). Micelles are prepared in toluene stock solution at a polymer concentration of 5 mg/mL, which is diluted in subsequent processing steps. The inorganic precursor is added to the polymer solution in equimolar amounts with respect to the number of pyridine units and stirred vigorously on a hot plate at a temperature of 50 °C for 24 h. The inorganic precursor is then reduced to metallic nanoparticles by adding a reduction agent (e.g., sodium boron-hydride ($NaBH_4$, Aldrich, 95% purity) to the micellar solution. The formation of metallic nanoparticles is indicated by a color change of the solution. X-ray diffractometry (not shown), XPS and TEM analysis are performed to evaluate the particle size, crystal structure and chemical composition. In the case of Au nanoparticles the reduction yields small, crystalline nanoparticles with fcc crystal structure (space group $Fm\bar{3}m$) and a lattice spacing of d_{100}= 4.08 Å. The formation of crystalline Co/CoO nanoparticles is achieved using super hydride reduction[46,47] in lithium boron-hydride ($LiBH_4$) at elevated temperatures (80 °C). In contrast to the gold precursor ($HAuCl_4$), which is

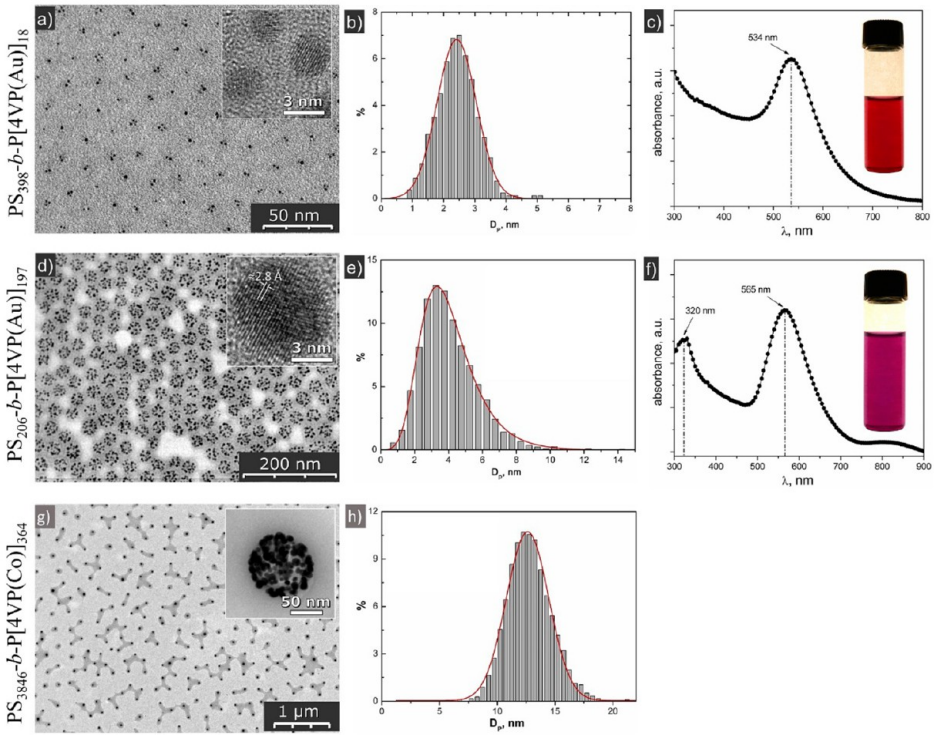

Figure 2. (a) TEM micrographs of gold nanoparticles stabilized in the core of PS_{398}-*b*-$P4VP_{18}$ micelles; the inset shows a HR-TEM micrograph of the particles. (b) Histogram of the particle size distribution as determined from TEM micrographs. (c) UV−vis absorption spectra of PS_{398}-*b*-$P4VP_{18}$ micelles incorporating Au nanoparticles in their core; the inset is an optical photograph of the nanoparticles in toluene solution. (d) TEM micrographs of gold nanoparticles stabilized in the core of PS_{206}-*b*-$P4VP_{197}$ micelles; the inset shows a HR-TEM micrograph of the particles; the spacing of the fringes estimated in HR-TEM is 2.8 Å. (e) Histogram of the particle size distribution as determined from TEM micrographs. (f) UV−vis absorption spectra of PS_{206}-*b*-$P4VP_{197}$ micelles incorporating Au nanoparticles in their core; the inset is an optical photograph of the nanoparticles in toluene solution. (g) TEM micrographs show Co nanoparticles incorporated in the micelle's core of PS_{3846}-*b*-P[4VP(Co)]$_{364}$ micelles. (h) Histogram of the particle corresponding size distribution.

DOI: 10.1021/am5076056
ACS Appl. Mater. Interfaces 2015, 7, 12440−12449

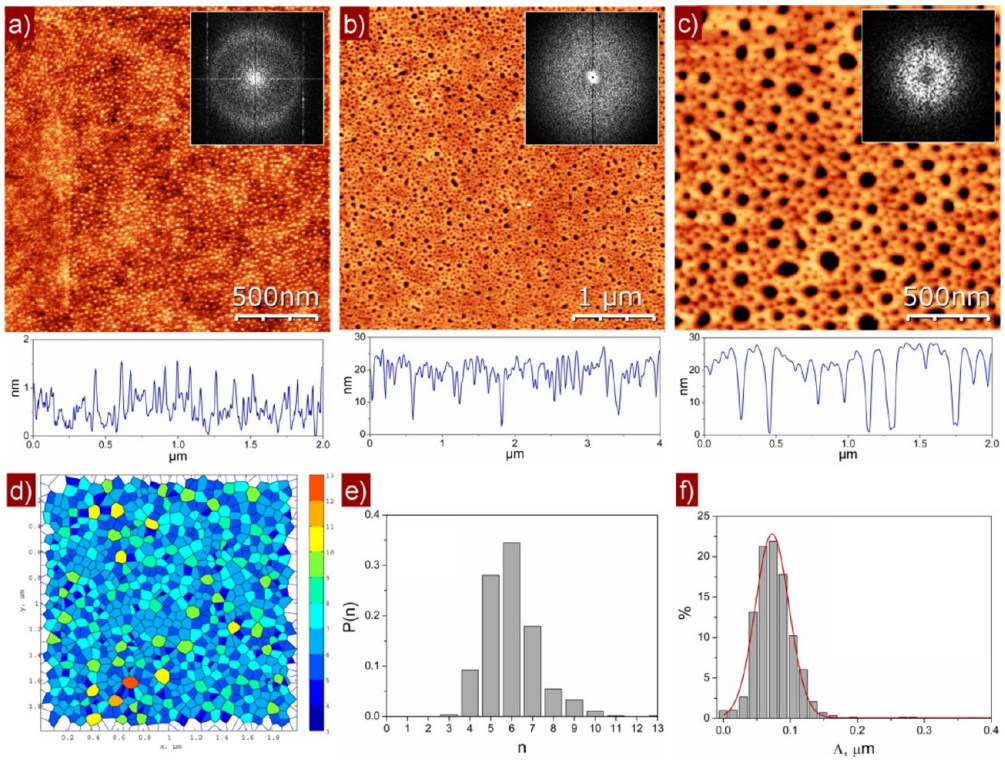

Figure 3. AFM topographies of (a) hexagonally ordered and (b, c) nanoporous films obtained via directed self-assembly of PS_{389}-*b*-P[4VP(Au)]$_{18}$ micelles. (d) The color-coded Voronoi diagram of the nanoporous film reveals (e) a preferred 6-fold coordination of the pores and (f) an average spacing of 73 nm.

easily reduced, the complete reduction of $CoCl_2$ requires a high excess of reducing agent. Such high excess concentrations also lead to morphological changes in the micelle solution as well as the deposited films. Therefore, here we use only a 3-fold excess of $LiBH_4$ with respect to Co ions, which yields an incomplete reduction. The formation of Co NPs is indicated by a color change of the solution to dark gray upon the addition of the reducing agent. However, residual precursor is left in the micelle core and can be completely reduced after film deposition. In this case, as an alternative to chemical reduction in solution, which involves the addition of a reducing agent, the inorganic precursors is reduced by exposing nanostructured hybrid materials in thin film to UV irradiation for Au or a reactive plasma (O*, H*) as confirmed via XPS measurements. In Table 1, details on the polymers and nanoparticle synthesis used herein are summarized.

Dynamic light scattering (DLS) (M802 DLS, Viscotek) measurements confirmed the presence of uniform micelles with a hydrodynamic radius (R_H) in a selective solvent (toluene) for the PS block. Transmission electron microscopy (TEM) measurements were performed to investigate the microstructure of metallic nanocrystals, synthesized within the micelle core. Both, the crystallinity and size distribution, were evaluated. Figure 2a shows typical TEM micrographs recorded in a TECNAI Biotwin (FEI Ltd.) of metal loaded PS-*b*-P4VP micelles with different molecular weights and volume fraction, where metal nanoparticles appear as dark spots in the image. The PS-*b*-P4VP block copolymer provides excellent control over the size and the polydispersity of the nanoparticles (NPs). As a result, nanoparticles with a narrow diameter distribution are formed within the micelle core (P4VP), whereas the surrounding PS shell stabilizes the particles and prevents coagulation.

The TEM micrographs in Figure 2a, d, g reveal that metal nanoparticles with diameters in the range of 2−3 nm were synthesized within the PS_{398}-*b*-$P4VP_{18}$ micelle core and larger particles of 4−5 nm and 10−15 nm were obtained for PS_{206}-*b*-$P4VP_{197}$ and PS_{3846}-*b*-$P4VP_{364}$, respectively. Additionally, HR-TEM measurements were performed on a JEOL JEM-2110F operated at 200 kV. The existence of the fringes in HR-TEM micrograph (insets Figure 2a, d) signifies the existence of single crystalline Au particles. The analysis of the fringe pattern in Figure 2d yields a lattice spacing of approximately 2.8 Å, which corresponds to the (110) bulk lattice spacing of gold and confirms the formation of crystalline metal nanoparticles within the micelle core. The histograms of the particle size-distributions (Figure 2b, e) as determined from TEM measurements reveals a mean particle diameter of 2.4 nm with a standard deviation of 0.6 nm for PS_{398}-*b*-$P4VP_{18}$, while larger particles Au of 3.6 ± 1.5 nm are obtained for PS_{206}-*b*-$P4VP_{197}$. Because of their low polydispersity, the Au nanoparticles exhibit distinct optical absorption properties. Figure 2c,f shows UV−vis absorption spectra of the nanoparticles stabilized in the core of PS-*b*-P4VP micelles. The absorption band at λ = 534 and 565 nm, because of the surface plasmon resonance effect, is characteristic for small Au nanoparticles (<5 nm).[48] The presence of a single, narrow absorption band also signifies that uniform, noninteracting Au nanoparticles are prepared within the core of PS-*b*-P4VP micelles in toluene. The characteristic absorption behavior of these nanoparticles in the visible spectrum leads to the typical ruby-red color of colloidal gold (inset Figure 2c, f). The observation of a weak absorption band at λ= 320 in Figure 2f indicates the presence of small amounts of residual $HAuCl_4$ precursor in the solution after chemical reduction. Micelles of PS_{206}-*b*-$P4VP_{197}$ with a large P4VP volume fraction can coordinate a high quantity of precursor. Though a complete chemical reduction can be achieved, the addition of large excess of reducing agent ($NaBH_4$) leads to structural changes due to the high ion concentration of the solution. In Figure 2c this peak is absent, because the relatively small concentration of inorganic precursor can be completely reduced within the micelle core without triggering morphological changes.

In the case of Co nanoparticles synthesized within the micelle's core, the high polydispersity of the PS_{3846}-*b*-$P4VP_{364}$ block copolymer manifests itself in the broad size-distribution. The TEM micrographs (Figure 2g) reveal Co nanoparticles that enrich at the interface between the P4VP core and the PS shell of PS_{3846}-*b*-$P4VP_{364}$ micelles in toluene; the corresponding histogram of the particle size-

DOI: 10.1021/am5076056
ACS Appl. Mater. Interfaces 2015, 7, 12440−12449

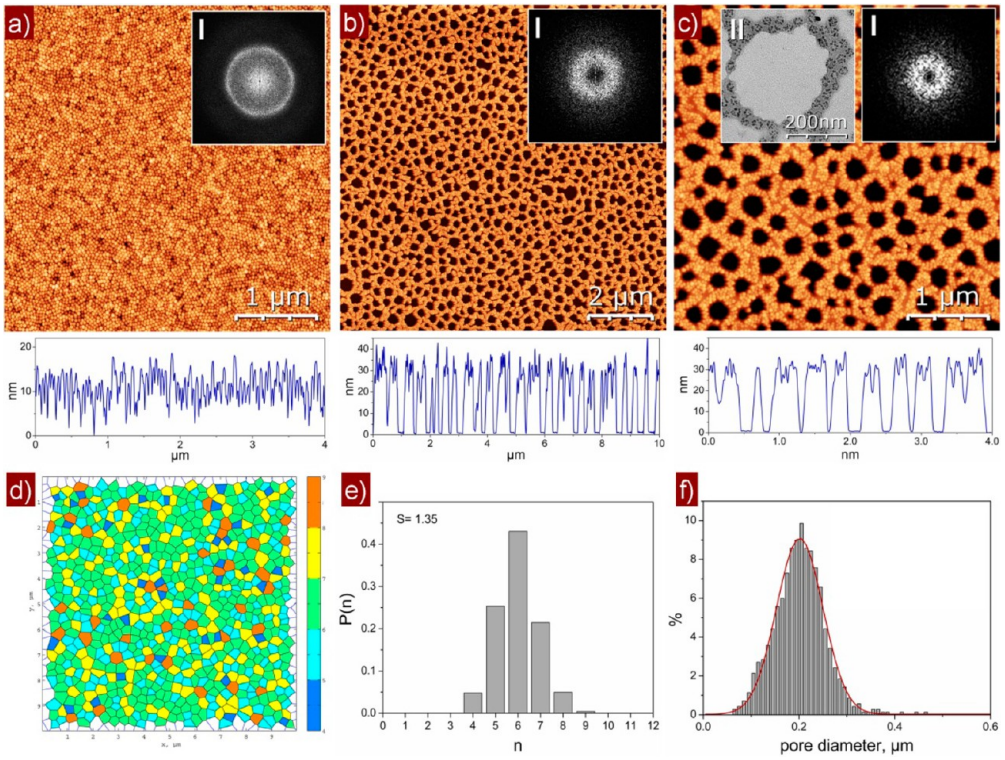

Figure 4. AFM topographies of (a) hexagonally ordered and (b, c) nanoporous films obtained via directed self-assembly of PS_{206}-*b*-P[4VP(Au)]$_{197}$ micelles. (d) The color-coded Voronoi diagram of nanoporous films reveals (e) a preferential 6-fold coordination of the pores and (f) an average pore diameter of 195 nm.

distribution (Figure 2h) yields a mean particle size of 12.8 nm with a standard deviation of 2.1 nm

RESULTS AND DISCUSSION

Spin-coating solutions of nanoparticles stabilized with PS-*b*-P4VP block copolymers onto solid substrates can be used to fabricate regular nanostructures in thin film. Usually, the deposition of micellar aggregates of PS-*b*-P[4VP(Au)] leads to hexagonally ordered patterns (Figure 3a) of close-packed micelles. The structure formation is driven by the solvent evaporation from the top of the fluid film during spin-coating, but other factors have to be considered as well. Recently, it was shown that the molecular parameters of the block copolymer, in particular the initial polymer concentration, the type of solvent, and the substrate, can be used as "tools" to control the structure formation in thin film by balancing competing interactions, such as wetting/dewetting, microphase separation, and instabilities of the fluid film during solvent evaporation.[32,49] Hence, nonhexagonally ordered patterns can be obtained via spin-coating of metal-loaded PS-*b*-P4VP micelles under appropriate conditions.

1. Nanoporous Thin Films. Balancing the intermicellar interactions as well as the wetting/dewetting competitions with the substrate surface through the optimal combination of influencing parameters holds the key for fabricating well-ordered nanoporous structures with a specific pore diameter. Preferential swelling of the PS and P4VP block with the solvents (toluene and THF) can lead to heterogeneous evaporation from the film surface. Additionally, THF swells the micelle's P4VP core and preferentially wets the substrate surface, whereas PS and toluene dewet the substrate and enrich at the free surface, because of the lower surface energy of PS.[25,26] As a result, dewetting of coronal PS chains on the hydrophilic substrate, swelling of the micelle's P4VP core and the complex interplay[27−31] of interfacial interactions together with successive solvent evaporation from the film surface are tuned to engineer nanoporous morphologies of PS-*b*-P[4VP-(Au)] hybrid materials.

As a consequence, nanoporous thin films are obtained via evaporation-induced self-assembly after adding a second, nonselective cosolvent (THF) to the toluene solution in a ratio of THF:toluene =1:2, followed by the adsorption of micelles on hydrophilic SiO_2 substrates (Figure 3b). No additional treatment has to be applied to develop the porous structure after the film deposition process. The film represents an array of heterogeneous, nanoporous domains oriented normally to the substrate (Figure 3c). Analysis of the cross-sectional profile reveals the depth of the nanopores to be (28 ± 4) nm, which corresponds to the film thickness. Therefore, it can be assumed that the porous structure completely penetrates the film to the substrate surface.

Different sizes of nanoporous morphologies are observed, which can be classified into two different types. The Voronoi diagram in Figure 3d reveals the presence of large holes (~120 nm), which are constantly surrounded by small pores (~25 nm). Analysis of the nearest-neighbor distribution (Figure 3e) shows that the pores tend to form hexagonally ordered patterns. However, the existence of different pore diameters perturbs the hexagonally ordered structure and results in local, short-range order. The pore density is approximately 35% as determined from AFM topography data. With the given distribution of pore diameters, this translates into an order of magnitude of 10^{10} pores/cm^2; the average spacing of the pores is approximately 73 nm (Figure 3f)

DOI: 10.1021/am5076056
ACS Appl. Mater. Interfaces 2015, 7, 12440−12449

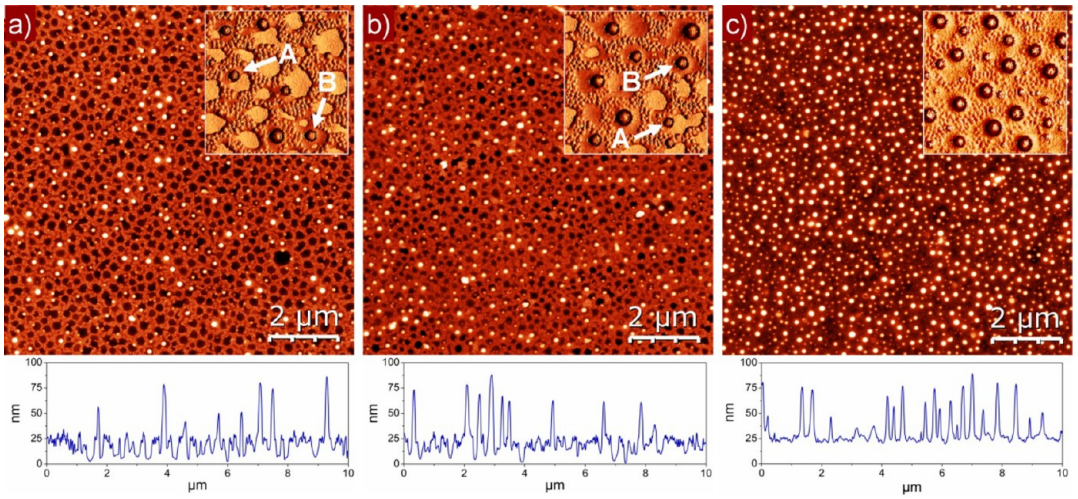

Figure 5. AFM topographies of PS_{3846}-*b*-P[4VP(Co)]$_{364}$ micelles deposited on nanoporous templates of PS_{206}-*b*-P[4VP(Au)]$_{197}$ at concentrations of (a) 1, (b) 2, and (c) 4 mg/mL. The insets are AFM phase images signifying the increasing coverage of pores with micelles as the polymer concentration of the coating solution increases.

The characteristic dimensions of hexagonally ordered arrays of spherical PS-*b*-P[4VP(Au)] micelles are determined by the molecular weight and volume fraction of the block copolymer. This gives rise to the assumption that also the critical length scale of nanoporous films fabricated via directed self-assembly of PS-*b*-P[4VP(Au)] micelles also depends on the molecular parameters of the block copolymer. Hence, changing the molecular weight and volume fraction of the block copolymer can provide control over the pore diameter, pore density, and spacing between the pores. Moreover, since the nanoparticles are synthesized in situ within the micelle's core, the micellar morphology effectively stabilizes the nanoparticles and allows tuning the particle size. Therefore, substituting the diblock copolymer PS_{398}-*b*-P[4VP(Au)]$_{18}$ with PS_{206}-*b*-P[4VP(Au)]$_{197}$ to fabricate nanoporous structures in spin-coated thin films not only allows changing the pore diameter but also affects the particle size.

Adsorbing micelles of PS_{206}-*b*-P[4VP(Au)]$_{197}$ from toluene solution onto solid substrates yields the typical hexagonally ordered patterns of densely packed micelles (Figure 4a). However, nanoporous thin films (Figure 4b, c) can be prepared in exactly the same way as demonstrated previously for PS_{398}-*b*-P[4VP(Au)]$_{18}$ by adding a nonselective cosolvent (THF) to the solutions prior to film deposition. The difference is that the characteristic dimensions of the porous nanostructures change, due to the higher volume fraction of P4VP in the case of PS_{206}-*b*-P[4VP(Au)]$_{197}$. The pores are again continuous through the film having a depth of 33 nm. Moreover, the presence of a ring in the corresponding 2D-FFT image (inset I Figure 4b, c) signifies an isotropic structure with a dominant length scale of 260 nm compared to 73 nm in the case of PS_{398}-*b*-P[4VP(Au)]$_{18}$. In analogy to previous observations, the porous structure is formed though directed self-assembly of PS_{206}-*b*-P[4VP(Au)]$_{197}$ micelles, which act as building blocks, via controlled dewetting of PS coronal chains on the hydrophilic SiO_2 substrates. The corresponding TEM micrograph (inset II Figure 4c) shows the spatial distribution of Au nanoparticles in the porous film.

The regularity of nanoporous films on Si substrates is again evaluated by means of Voronoi tessellation; a typical Voronoi diagram is shown in Figure 4d. The results indicate a good short-range order with a 6-fold coordination of the pores (Figure 4e). However, the patterns are isotropic on a macroscopic length scale because of the low degree of long-range order. In particular, the coordination number (n) varies between 4 and 8 for nanoporous films fabricated using PS_{206}-*b*-P[4VP(Au)]$_{197}$ micelles. The average pore diameter is 195 nm (Figure 4f) and the total pore density is approximately 8×10^8 pores/cm^2. Hence, changing the molecular weight and volume fraction of the block copolymer provides control over the pore diameter.

2. Binary Nanoparticle Superlattices. Nanostructured hybrid materials are promising candidates for the fabrication of functional devices with unique optical, electronic or catalytic properties. The range of potential applications of these materials can be greatly expanded if truly functional nanostructures based on multiple components can be fabricated. Thus, the self-assembly of two different types of nanoparticles into ordered binary nanoparticle superlattices can provide a generic path to a large variety of functional materials with precisely controlled chemical composition and well-defined spatial arrangement of the components.[32,33] The self-assembly of particle superlattices is usually determined by noncovalent interactions, such as hydrogen bonding, dipole–dipole, electrostatic, van der Waals, and hydrophobic interactions among the nanoparticle building blocks. In the past, these interactions were tuned to produce well-defined particle assemblies via electric-field- and template-assisted self-assembly.[34−39] Recently, Shevchenko et al.[40] demonstrated the fabrication of a number of long-range ordered binary nanoparticle superlattices by tuning the steric- and electrostatic interactions among different types of nanoparticles. Despite its underlying success, the fabrication of multifunctional materials via assembly of colloidal particles faces numerous challenges in terms of scalability, diversity and control over the structure formation.[41] An alternative way to overcome these issues is to use different types of polymer templated nanoparticles to create ordered, binary particle arrays by tuning the self-assembly of the organic components.[42−44] Herein, we explore this possibility to fabricate bimetallic particle assemblies via directed self-assembly of metal-loaded PS-*b*-P4VP block copolymer micelles. The general concept is illustrated in Figure 1c. First, block

DOI: 10.1021/am5076056
ACS Appl. Mater. Interfaces 2015, 7, 12440−12449

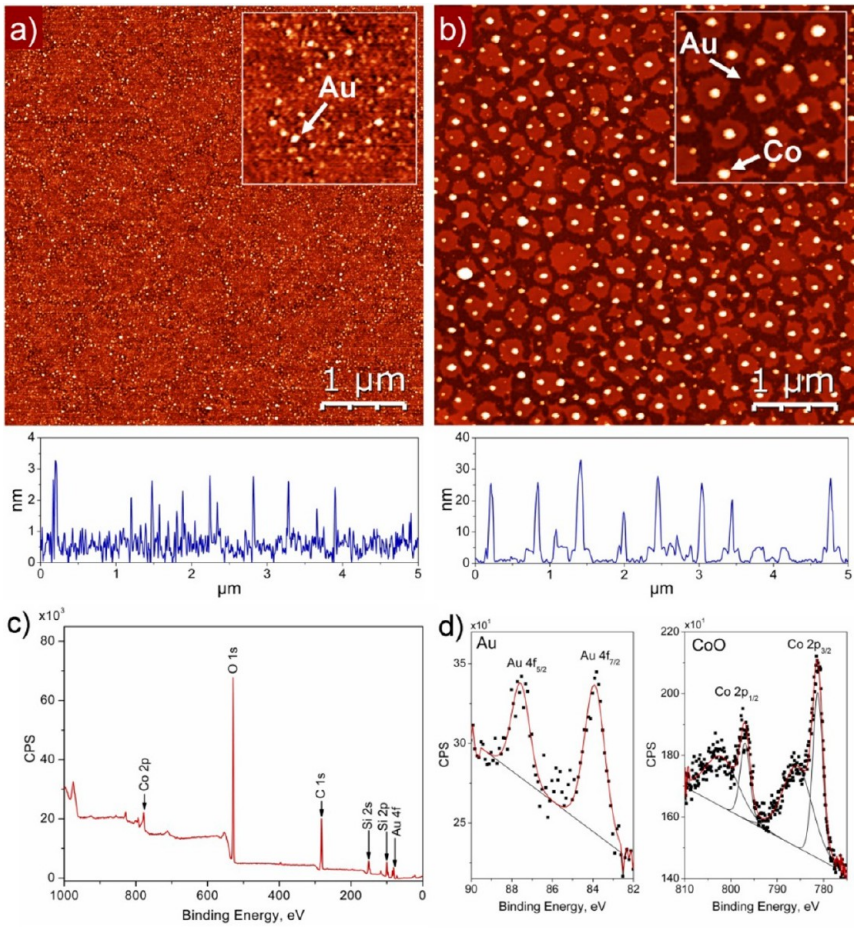

Figure 6. AFM topographies of (a) porous templates PS_{206}-*b*-P[4VP(Au)]$_{197}$ after oxygen plasma etching and (b) binary superlattices of Au and Co nanoparticles after loading the templates with PS_{3846}-*b*-P[4VP(Co)]$_{364}$ followed by oxygen plasma etching. The insets are magnified AFM height images of the nanoparticle structures. (c) XPS spectra of binary Au and Co particle assemblies on SiO_2 substrates; (d) high-resolution XPS spectra of the Au-4f and Co-2p regions.

copolymer micelles incorporating Au nanoparticles in their P4VP core are used to generate well-defined nanoporous structures in self-assembled thin films as described above. These patterns are then used as topographic templates for the deposition of PS_{3846}-*b*-P[4VP(Co)]$_{364}$ micelles (Figure 5) incorporating a different type of nanoparticle, e.g. cobalt (Co). The average intermicellar spacing in these films is 297 nm with a micellar bump height of 83 nm. Micellar films of PS_{3846}-*b*-P[4VP(Co)]$_{364}$ show relatively poor long-range order and micelles with significantly different sizes can be found. The reason is the unusually high polydispersity of the PS_{3846}-*b*-$P4VP_{364}$ block copolymer of M_w/M_n = 1.37. Only polymer chains with comparable molecular weight can self-assemble into micelles, which leads to a broad distribution of micelle diameters. Irregular structures are obtained upon deposition of these polydisperse micelles onto solid substrates, since space-filling arguments prevent the formation of long-range ordered hexagonal assemblies. If the critical dimensions (pore diameter) of the porous templates are compatible to the hydrodynamic radius of the cobalt-loaded micelles, they can be deposited in the center of each pore. Besides the necessity to control the dimension of the porous template, the degree of filling of the porous template can be controlled through the number of micelles deposited into the template, e.g., the solution concentration, see Figure (Figure 5a–c). As a result, the cobalt-loaded micelles are located preferentially within the pores of the templating layer.

The degree of occupation depends on the polymer concentration in the casting solution of PS_{3846}-*b*-P[4VP-(Co)]$_{364}$. At low initial concentrations the template is only partially filled (Figure 5 a, b). Complete filling of the porous template can be achieved once a certain concentration threshold is reached (Figure 5c), which is below the concentration to form micellar monolayers on plain substrates, but the exact value depends on the pore size and -density of the template. Hence, the polymer concentration can be controlled to adjust the surface coverage of the micellar film to match the pore density of the porous templates. In the case of PS_{3846}-*b*-P[4VP(Co)]$_{364}$ micelles deposited into porous templates of PS_{206}-*b*-P[4VP(Au)]$_{197}$, the threshold concentration is approximately 3.5 mg/mL. At higher initial polymer concentrations, the templating layer is increasingly overloaded and a larger fraction of the micelles is located on top of the porous template rather than within the pores. The insets in Figure 5a–c are AFM phase images of the films signifying the increasing degree of filling and the location of micelles within the porous structure at different concentrations of the casting solution. It can be noted that a large fraction of micelles is located at the edge of the pores (arrow A), whereas the center position (arrow B) is occupied only if the size of the micelle matches the particular pore diameter. Moreover, the edges sites are the

DOI: 10.1021/am5076056
ACS Appl. Mater. Interfaces 2015, 7, 12440–12449

preferentially occupied to minimize the contact area of hydrophobic PS chains with the hydrophilic SiO_2 substrate, while maximizing the number of PS contacts among coronal PS chains of the templating layer and the micelles within the pores.

In the last step, the organic components can be extracted via calcination at high temperatures or oxygen plasma etching. The plasma cleaner (FEMTO, Diener Electronic, Nagold, Germany) was operated at 0.3mbar pressure and 18 sccm flow of pure oxygen (BOC, Nottingham, UK) for 120s at a power of 65 W to completely strip the PS-*b*-P4VP copolymer matrix. As a result, bimetallic assemblies of inorganic Au and Co nanoparticles are obtained, which mimic the morphology of the self-assembled block copolymer structures (Figure 6). The Au particles represent the order of the porous template (Figure 6a). The cross-sectional height profile obtained from AFM measurements suggests that the particles are below 3 nm in diameter, which is smaller than the size determined by TEM prior to the etching process. These results may indicate that the plasma etching process is not completely selective for the organic components, e.g. the diblock copolymer, but partially removes the inorganic components as well. A slow etching of the inorganic components can be observed under mild etching conditions, where the material removal is dominated by chemical etching with oxygen radicals (O*) and physical etching (sputtering) is comparably weak.

Removing the organic matrix via oxygen plasma etching from porous templates of PS_{206}-*b*-$P[4VP(Au)]_{197}$ after depositing micelles of PS_{3846}-*b*-$P[4VP(Co)]_{364}$ within the pores leads to bimetallic surface structures of Au and Co nanoparticles (Figure 6b).

Again the Au nanoparticles mimic the structure of the porous template, whereas the Co particles are located in the pores, surrounded by smaller Au particles. In fact, each pore contains at least one Co nanoparticle; these are, however, not necessarily found in the center of the pores. Because of the larger size of the PS_{206}-*b*-$P[4VP(Au)]_{197}$ and PS_{3846}-*b*-$P[4VP(Co)]_{364}$ structures, i.e., the micellar bump height, longer etching times are required to remove block copolymer form the Co loaded PS_{3846}-*b*-$P[4VP]_{364}$ micelles. As a result, the patterns of inorganic Au nanoparticles are increasingly influenced by the etching process. Additionally, during the etching process a thicker SiO_2 layer may grow due to oxidation of the Si substrate beneath the natural oxide. The growing oxide layer can be noted as brighter patches around the cobalt nanoparticles in the porous structure in Figure 6b, whereas the Au nanoparticles appear darker signifying a lower height. Additional XPS measurements (Figure 6c, d) reveal that both Au and Co nanoparticles are present on the SiO_2 substrate, while no trace of Cl atoms are detected that would indicate residual inorganic precursor incorporated in the micelle's core. The C 1s signal decreases during the etching process, indicating the extraction of the organic matrix. However, the presence of a remaining C 1s signal after plasma etching the samples under mild conditions (60s @ 18 sccm O_2, 40W) signifies the presence of residual polymer layer on the substrates. The high resolution XPS scans of both the Au-4f and the Co-2p region are shown in Figure 6d. Component analysis of these spectra indicates that indeed metallic Au nanoparticles are present on the substrate, although the signal is weak because of the low volume fraction of the nanoparticles, partial removal of Au during the etching process, and Au particles buried beneath a growing SiO_2 layer. Furthermore, the Co-2p signal carries the typical signature of cobalt-oxide nanoparticles (CoO).[50] In order to obtain metallic Co nanoparticles one has to find a way to protect the particles from oxidation, either by etching with hydrogen plasma, UV degradation of the polymer, or using the polymer film as a protective layer.

In principle, our simple multistep self-assembly approach can be applied to fabricate well-ordered nanostructures based on a wide range of inorganic components, including metals, semiconductors, and magnetic nanoparticles, provided that they can be stabilized in the core of block copolymer micelles.

CONCLUSIONS

In the present study, a versatile method is demonstrated to fabricate hierarchical nanoporous films and bimetallic nanostructures via directed self-assembly of block copolymer/nanoparticle hybrid materials. First, gold nanoparticles stabilized within the core of polystyrene-*block*-polyvinylpyridine (PS-*b*-P4VP) micelles are prepared using a templating approach in toluene solution. Different molecular weight of the PS-*b*-P4VP block copolymers and a nonselective cosolvent are used to generate hierarchical nanoporous structures with controlled pore diameter via spin-casting of micellar solutions onto hydrophilic substrates. The porous films can be used to template the deposition of a second type of micelles, whose core is loaded with another metal, e.g. cobalt (Co). The critical factor is matching the hydrodynamic radius of the micelles with the pore radius. If this condition is not fulfilled, the micelles are preferentially located at the edge of the pores. Purely inorganic, bimetallic nanostructures containing Au and Co/CoO nanoparticles are obtained after extraction of the block copolymer via calcination or oxygen plasma treatment. The resulting metallic structures mimic the original film morphology, where Co/CoO nanoparticles are located at the center of the pores surrounded by a large number of small Au particles. It is important to note that this concept can then be applied in a generic way to fabricate ordered nanostructures with different combinations of inorganic materials in binary particle assemblies. Therefore, these ordered nanoporous structures based on block copolymers and different types of inorganic nanoparticles possess great potential in many applications including membranes, catalysis, optical coatings, and electronics, among many other examples.

AUTHOR INFORMATION

Corresponding Authors

*E-mail: Torsten.Pietsch@uni-konstanz.de. Tel: +49(0)7531 883861. Fax: +49(0)7531 883090.

*E-mail: amir.fahmi@hochschule-rhein-waal.de. Tel: +49(0) 2821 80673634. Fax: +49(0)2821 80673162.

Present Addresses

‡T.P. is currently at Fachbereich Physik, Universität Konstanz, Universitätsstraße 10, D-78464 Konstanz, Germany

#A.F. is currently at Rhine-Waal University of Applied Sciences, Marie-Curie-Straße 1, D-47533 Kleve, Germany

Notes

The authors declare no competing financial interest.

ACKNOWLEDGMENTS

This work was funded by the UK EPSRC through the Nottingham IMRC. P.M.-B. acknowledges funding by the Nanosystems Initiative Munich (NIM).

DOI: 10.1021/am5076056
ACS Appl. Mater. Interfaces 2015, 7, 12440−12449

REFERENCES

(1) Ibn-Elhaj, M.; Schadt, M. Optical Polymer Thin Films with Isotropic and Anisotropic Nano-Corrugated Surface Topologies. *Nature* **2001**, *410*, 796−799.

(2) Walheim, S.; Schäffer, E.; Mlynek, J.; Steiner, U. Nanophase-Separated Polymer Films as High-Performance Antireflection Coatings. *Science* **1999**, *283*, 520−522.

(3) Joo, S. H.; Choi, S. J.; Oh, I.; Kwak, J.; Liu, Z.; Terasaki, O.; Ryoo, R. Ordered Nanoporous Arrays of Carbon Supporting High Dispersions of Platinum Nanoparticles. *Nature* **2001**, *412*, 169−172.

(4) Nair, B. N.; Suzuki, T.; Yoshino, Y.; Gopalakrishnan, S.; Sugawara, T.; Nakao, S.; Taguchi, H. An Oriented Nanoporous Membrane Prepared by Pulsed Laser Deposition. *Adv. Mater.* **2005**, *17*, 1136−1140.

(5) Shiflett, M. B.; Foley, H. C. Ultrasonic Deposition of High-Selectivity Nanoporous Carbon Membranes. *Science* **1999**, *285*, 1902−1905.

(6) Chang, H.; Kosari, F.; Andreadakis, G.; Alam, M. A.; Vasmatzis, G.; Bashir, R. DNA-Mediated Fluctuations in Ionic Current through Silicon Oxide Nanopore Channels. *Nano Lett.* **2004**, *4*, 1551−1556.

(7) Fu, G. D.; Kang, E. T.; Neoh, K. G. Three-Dimensionally Ordered Porous Membranes Prepared Via Self-Assembly and Reverse Micelle Formation from Well-Defined Amphiphilic Block Copolymers. *Langmuir* **2005**, *21*, 3619−3624.

(8) Fu, G. D.; Yuan, Z. L.; Kang, E. T.; Neoh, K. G.; Lai, D. M.; Huan, A. C. H. Nanoporous Ultra-Low-Dielectric-Constant Fluoropolymer Films Via Selective Uv Decomposition of Poly(Pentafluorostyrene)-Block-Poly(Methyl Methacrylate) Copolymers Prepared Using Atom Transfer Radical Polymerization. *Adv. Funct Mater.* **2005**, *15*, 315−322.

(9) Tian, Y.; Tatsuma, T. Mechanisms and Applications of Plasmon-Induced Charge Separation at Tio2 Films Loaded with Gold Nanoparticles. *J. Am. Chem. Soc. J. Am. Chem. Soc.* **2005**, *127*, 7632−7637.

(10) Bal, M.; Ursache, A.; Tuominen, M. T.; Goldbach, J. T.; Russell, T. P. Nanofabrication of Integrated Magnetoelectronic Devices Using Patterned Self-Assembled Copolymer Templates. *Appl. Phys. Lett.* **2002**, *81*, 3479−3481.

(11) Wang, Y. J.; Yu, A. M.; Caruso, F. Nanoporous Polyclectrolyte Spheres Prepared by Sequentially Coating Sacrificial Mesoporous Silica Spheres. *Angew. Chem. Int. Edit* **2005**, *44*, 2888−2892.

(12) Ham, H. T.; Chung, I. J.; Choi, Y. S.; Lee, S. H.; Kim, S. O. Macroporous Polymer Thin Film Prepared from Temporarily Stabilized Water-in-Oil Emulsion. *J. Phys. Chem. B* **2006**, *110*, 13959−13964.

(13) Imhof, A.; Pine, D. J. Ordered Macroporous Materials by Emulsion Templating. *Nature* **1997**, *389*, 948−951.

(14) Xu, L. G.; Geng, Z.; He, J. H.; Zhou, G. Mechanically Robust, Thermally Stable, Broadband Antireflective, and Superhydrophobic Thin Films on Glass Substrates. *ACS Appl. Mater. Interaces* **2014**, *6*, 9029−9035.

(15) Lee, J. W.; Ye, B. U.; Kim, D. Y.; Kim, J. K.; Heo, J.; Jeong, H. Y.; Kim, M. H.; Choi, W. J.; Baik, J. M. Zno Nanowire-Based Antireflective Coatings with Double-Nanotextured Surfaces. *ACS Appl. Mater. Interfaces* **2014**, *6*, 1375−1379.

(16) Galeotti, F.; Trespidi, F.; Timo, G.; Pasini, M. Broadband and Crack-Free Antireflection Coatings by Self-Assembled Moth Eye Patterns. *ACS Appl. Mater. Interfaces* **2014**, *6*, 5827−5834.

(17) Singh, S. K.; Singh, A. K.; Aranishi, K.; Xu, Q. Noble-Metal-Free Bimetallic Nanoparticle-Catalyzed Selective Hydrogen Generation from Hydrous Hydrazine for Chemical Hydrogen Storage. *J. Am. Chem. Soc.* **2011**, *133*, 19638−19641.

(18) Soule, J. F.; Miyamura, H.; Kobayashi, S. Powerful Amide Synthesis from Alcohols and Amines under Aerobic Conditions Catalyzed by Gold or Gold/Iron, -Nickel or -Cobalt Nanoparticles. *J. Am. Chem. Soc.* **2011**, *133*, 18550−18553.

(19) Jin, P. Y.; Liang, X.; He, Y. H.; Liu, S. J.; Zhu, X. L. Compositionally Controlled Self-Assembly of Hierarchical Pd-Ni Bimetallic Chains. *Eur. J. Inorg. Chem.* **2014**, 4144−4150.

(20) Chen, H. Y.; Li, Y.; Zhang, F. B.; Zhang, G. L.; Fan, X. B. Graphene Supported Au-Pd Bimetallic Nanoparticles with Core-Shell Structures and Superior Peroxidase-Like Activities. *J. Mater. Chem.* **2011**, *21*, 17658−17661.

(21) Suntivich, J.; Xu, Z. C.; Carlton, C. E.; Kim, J.; Han, B. H.; Lee, S. W.; Bonnet, N.; Marzari, N.; Allard, L. F.; Gasteiger, H. A.; Hamad-Schifferli, K.; Shao-Horn, Y. Surface Composition Tuning of Au-Pt Bimetallic Nanoparticles for Enhanced Carbon Monoxide and Methanol Electro-Oxidation. *J. Am. Chem. Soc.* **2013**, *135*, 7985−7991.

(22) Zhang, H. J.; Haba, M.; Okumura, M.; Akita, T.; Hashimoto, S.; Toshima, N. Novel Formation of Ag/Au Bimetallic Nanoparticles by Physical Mixture of Monometallic Nanoparticles in Dispersions and Their Application to Catalysts for Aerobic Glucose Oxidation. *Langmuir* **2013**, *29*, 10330−10339.

(23) Zhu, Y.; Zhang, S. R.; Ye, Y. C.; Zhang, X. Q.; Wang, L.; Zhu, W.; Cheng, F.; Tao, F. Catalytic Conversion of Carbon Dioxide to Methane on Ruthenium-Cobalt Bimetallic Nanocatalysts and Correlation between Surface Chemistry of Catalysts under Reaction Conditions and Catalytic Performances. *ACS Catal.* **2012**, *2*, 2403−2408.

(24) Xu, C. X.; Liu, Y. Q.; Wang, J. P.; Geng, H. R.; Qiu, H. J. Fabrication of Nanoporous Cu-Pt(Pd) Core/Shell Structure by Galvanic Replacement and Its Application in Electrocatalysis. *Acs Appl. Mater. Inter* **2011**, *3*, 4626−4632.

(25) Lin, Y.; Boker, A.; He, J. B.; Sill, K.; Xiang, H. Q.; Abetz, C.; Li, X. F.; Wang, J.; Emrick, T.; Long, S.; Wang, Q.; Balazs, A.; Russell, T. P. Self-Directed Self-Assembly of Nanoparticle/Copolymer Mixtures. *Nature* **2005**, *434*, 55−59.

(26) Shin, K.; Leach, K. A.; Goldbach, J. T.; Kim, D. H.; Jho, J. Y.; Tuominen, M.; Hawker, C. J.; Russell, T. P. A Simple Route to Metal Nanodots and Nanoporous Metal Films. *Nano Lett.* **2002**, *2*, 933−936.

(27) Misner, M. J.; Skaff, H.; Emrick, T.; Russell, T. P. Directed Deposition of Nanoparticles Using Diblock Copolymer Templates. *Adv. Mater.* **2003**, *15*, 221−224.

(28) Kim, D. H.; Sun, Z. C.; Russell, T. P.; Knoll, W.; Gutmann, J. S. Organic-Inorganic Nanohybridization by Block Copolymer Thin Films. *Adv. Funct Mater.* **2005**, *15*, 1160−1164.

(29) Spatz, J. P.; Roescher, A.; Möller, M. Gold Nanoparticles in Micellar Poly(Styrene)-B-Poly(Ethylene Oxide) Films-Size and Interparticle Distance Control in Monoparticulate Films. *Adv. Mater.* **1996**, *8*, 337−340.

(30) Koh, H. D.; Kang, N. G.; Lee, J. S. Fabrication of an Open Au/Nanoporous Film by Water-in-Oil Emulsion-Induced Block Copolymer Micelles. *Langmuir* **2007**, *23*, 12817−12820.

(31) Pietsch, T.; Gindy, N.; Mahltig, B.; Fahmi, A. Fabrication of Functional Nano-Objects Via Self-Assembly of Nanostructured Hybrid Materials. *J. Polym. Sci., Part B: Polym. Phys.* **2010**, *48*, 1642−1650.

(32) Pietsch, T.; Metwalli, E.; Roth, S. V.; Gebhardt, R.; Gindy, N.; Muller-Buschbaum, P.; Fahmi, A. Directing the Self-Assembly of Mesostructured Hybrid Materials: Effect of Polymer Concentration and Solvent Type. *Macromol. Chem. Phys.* **2009**, *210*, 864−878.

(33) Fahmi, A.; Pietsch, T.; Mendoza, C.; Cheval, N. Functional Hybrid Materials. *Mater. Today* **2009**, *12*, 44−50.

(34) Gersappe, D. Modelling Micelle Formation in Confined Geometries. *High Perform Polym.* **2000**, *12*, 573−579.

(35) Leibler, L. Block Copolymers at Interfaces. *Phys. A* **1991**, *172*, 258−268.

(36) Cameron, N. S.; Corbierre, M. K.; Eisenberg, A. 1998 E.W.R. Steacie Award Lecture Asymmetric Amphiphilic Block Copolymers in Solution: A Morphological Wonderland. *Can. J. Chem.* **1999**, *77*, 1311−1326.

(37) Chu, B. Structure and Dynamics of Block-Copolymer Colloids. *Langmuir* **1995**, *11*, 414−421.

(38) Jain, S.; Bates, F. S. On the Origins of Morphological Complexity in Block Copolymer Surfactants. *Science* **2003**, *300*, 460−464.

(39) Pietsch, T.; Gindy, N.; Fahmi, A. Nano- and Micro-Sized Honeycomb Patterns through Hierarchical Self-Assembly of Metal-Loaded Diblock Copolymer Vesicles. *Soft Matter* **2009**, *5*, 2188−2197.

DOI: 10.1021/am5076056
ACS Appl. Mater. Interfaces 2015, 7, 12440−12449

(40) Nunes, S. P.; Behzad, A. R.; Peinemann, K. V. Self-Assembled Block Copolymer Membranes: From Basic Research to Large-Scale Manufacturing. *J. Mater. Res.* **2013**, *28*, 2661−2665.
(41) Yu, H. Z.; Qiu, X. Y.; Nunes, S. P.; Peinemann, K. V. Self-Assembled Isoporous Block Copolymer Membranes with Tuned Pore Sizes. *Angew. Chem., Int. Ed.* **2014**, *53*, 10072−10076.
(42) Fahmi, A.; Pietsch, T.; Gindy, N. Hierarchical Nanoporous Structures by Self-Assembled Hybrid Materials Based on Block Copolymers. *Macromol. Rapid Commun.* **2007**, *28*, 2300−2305.
(43) Chiu, J. J.; Kim, B. J.; Kramer, E. J.; Pine, D. J. Control of Nanoparticle Location in Block Copolymers. *J. Am. Chem. Soc.* **2005**, *127*, 5036−5037.
(44) Dixon, M. C.; Daniel, T. A.; Hieda, M.; Smilgies, D. M.; Chan, M. H. W.; Allara, D. L. Preparation, Structure, and Optical Properties of Nanoporous Gold Thin Films. *Langmuir* **2007**, *23*, 2414−2422.
(45) Müller-Buschbaum, P. Influence of Surface Cleaning on Dewetting of Thin Polystyrene Films. *Eur. Phys. J. E* **2003**, *12*, 443−448.
(46) Gual, A.; Godard, C.; Castillon, S.; Curulla-Ferre, D.; Claver, C. Colloidal Ru, Co and Fe-Nanoparticles. Synthesis and Application as Nanocatalysts in the Fischer−Tropsch Process. *Catal. Today* **2012**, *183*, 154−171.
(47) Sun, X. C.; Jia, Z. Y.; Huang, Y. H.; Harrell, J. W.; Nikles, D. E.; Sun, K.; Wang, L. M. Synthesis and Magnetic Properties of Copt Nanoparticles. *J. Appl. Phys.* **2004**, *95*, 6747−6749.
(48) Creighton, J. A.; Eadon, D. G. Ultraviolet Visible Absorption-Spectra of the Colloidal Metallic Elements. *J. Chem. Soc., Faraday Trans.* **1991**, *87*, 3881−3891.
(49) Müller-Buschbaum, P.; Bauer, E.; Wunnicke, O.; Stamm, M. The Control of Thin Film Morphology by the Interplay of Dewetting, Phase Separation and Microphase Separation. *J. Phys.: Condens. Mater.* **2005**, *17*, S363−S386.
(50) Coulter, K. E.; Sault, A. G. Effects of Activation on the Surface-Properties of Silica-Supported Cobalt Catalysts. *J. Catal.* **1995**, *154*, 56−64.

DOI: 10.1021/am5076056
ACS Appl. Mater. Interfaces 2015, 7, 12440−12449